J Therm Spray Tech
https://doi.org/10.1007/s11666-020-01125-3

PEER REVIEWED

Depositing Aluminum onto PEKK Composites by Cold Spray

P. Feng[1] · M. R. Rokni[1,2] · S. R. Nutt[1]

Submitted: 17 July 2020 / in revised form: 30 October 2020 / Accepted: 9 November 2020

Abstract High-pressure cold spray (HP-CS) was used to deposit aluminum onto polyetherketoneketone (PEKK) composite substrates. Aluminum powders were sprayed using N_2 and He carrier gas and a bond layer (BL) of commercial-purity Al (CP Al). Dense 7075 and CP Al deposits were achieved via combinations of BL-N_2, 7075/BL-N_2, and 7075/BL-He. Cold spray using 7075 Al particles or using He carrier gas yielded thinner deposits because of self-erosion and bond layer erosion. Substrate roughening was more severe when using He gas and generated more polymer debris at the deposit–substrate interface, yielding lower adhesive strength values between the deposit and the composite substrates. Adhesive strength depended on the bonding of initial particle layers that fused with the substrate.

Keywords adhesive strength · cold spray · deposition behaviors · interfacial microstructure · metallization of polymer composites · polymer–composite substrate

Introduction

To determine process conditions required to produce adherent metal deposits and understand powder–substrate interactions, the near-substrate microstructure of cold-sprayed (CS) metal on fiber-reinforced thermoplastic composites (FRTP) was investigated. Adhesion of deposits depends strongly on the interactions between the metal particles and the composite substrate, which affects the residual stress and microstructure at the deposit–substrate interface. Integration of metal coatings onto polymer composites through surface metallization could significantly broaden the use of thermoplastic composites, which is limited in some applications by low erosion resistance (Ref 1, 2) and electrical conductivity (Ref 3). Surface metallization can be an effective approach to bestow metallic properties and overcome these shortcomings, while retaining the high specific strength and modulus of the composite (Ref 4).

Different processes have been utilized to metallize composite surfaces, including physical vapor deposition (Ref 5), electroless plating (Ref 6), and thermal spray techniques, including high-velocity oxygen fuel (Ref 7) and plasma spraying (Ref 8). Although thermal spray techniques have greater deposition rates (Ref 9) compared to PVD, CVD, and electroplating processes, the feedstock powders are melted during deposition, with two adverse effects: deposits develop thermally induced residual stresses (and sometimes experience oxidation), and the molten droplets damage polymer substrates. For these reasons, thermal spray processes are incompatible with polymer and composite substrates (Ref 10-14). An alternative powder deposition process—cold spray—may be better suited to metal deposition onto heat-sensitive substrates.

Cold spray is a solid-state powder deposition process in which metal powders are accelerated via a supersonic gas flow to deposit onto substrates. Upon impact, the powders undergo severe plastic deformation (SPD) and effectively fuse (cold-weld) to produce a fully dense deposit. Recent studies have reported CS deposition onto polymer

✉ P. Feng
polunfen@usc.edu; brianfeng@alumni.usc.edu

[1] Department of Chemical Engineering and Materials Science, M.C. Gill Composites Center, University of Southern California, Los Angeles, CA, USA

[2] Present Address: Senior Aerospace SSP, Los Angeles, CA, USA

Published online: 30 November 2020

substrates (Ref 1, 2, 11-13, 15-26), and some of these have shown that thermoplastics are more compatible with CS, as thermosets either degrade or erode during deposition (Ref 15, 18, 20). In one study, thick and adherent CS deposits were produced on PEEK and PEI substrates (Ref 19). In that study, the CTE (coefficient of thermal expansion) match between deposit and substrate was important to obtaining adherent deposits. The present effort undertakes cold spray of Al powders onto a FRTP substrate (PEKK-30% short carbon fiber) for increased CTE compatibility with Al compared to other thermoplastics, as shown in Fig. 1 (Ref 27).

In this work, effects of materials and process parameters on CS Al metallization of a FRTP were investigated. Parameters varied included the effects of a compliant bond layer, powder hardness (CP Al versus 7075 Al), and carrier gas type. The relationship between microstructure and adhesive strength was investigated to better understand the deposit–substrate interaction and the deposit build-up process and characteristics. Experiments lay a foundation for a step change in metallization technology for weight savings and structural performance.

Experimental Methods

Polymer Composite Substrate

The substrate was injection-molded PEKK-30% short carbon fiber (KEPSTAN 8010C30, Arkema, Colombes, France). No surface preparation was performed prior to cold spraying. As shown in Fig. 1, the CTE of PEKK-30% CF differs from that of Al by only 57%, much less than the mismatch to PEEK, PEI, and ABS substrates (Ref 27). The similarity in CTE limits thermal stress in the deposit and reduces substrate distortion.

Feedstock Powders

Feedstock powders consisted of gas-atomized CP Al powder (99.9% commercial-purity Al, Alfa Aesar, Tewksbury, MA, USA) and 7075 Al powder (Ampel Inc, Elk Grove Village, IL, USA). The CP Al powder was deposited first to provide a compliant bond layer (interlayer) between the substrate and the 7075 Al particles. CP Al featured relatively low hardness and yield strength compared to 7075 Al, which featured greater strength and hardness. The powders were sieved with a no. + 270/− 635 wire mesh using a sieve shaker (AS 200 Analytical Sieve Shaker, Retsch GmbH, Germany), which yielded powder diameters of 20-53 µm. To remove moisture and increase powder flowability, the feedstock powders were dried in an oven at 100 °C prior to spraying.

Cold Spray Deposition

The 7075 and CP Al were deposited using a HP-CS system (VRC Gen III, VRC Metal Systems, Rapid City, SD, USA) using the cold spraying parameters reported previously (Ref 19). The pressure and temperature were maintained at 4.1 MPa and 350 °C at the heater exit. Cold spray was performed using a standoff distance of 75 mm, 90° deposition angle, medium powder feed rate (21.5 g/min), and a nozzle traveling speed of 350 mm/s. The CS gun consisted of a gas pre-chamber and a convergent–divergent accelerating nozzle with a throat diameter of 1.8 mm and an exit diameter of 7.8 mm. Powder was fed axially into the upstream of the nozzle from the back of the gun, and then, the accelerating gas was introduced into the pre-chamber. Details of the CS system have been reported (Ref 19). Initially, the feasibility of cold spray of CP Al onto FRTP was investigated by depositing with N_2. Subsequently, the effectiveness of using CP Al as a bond layer was evaluated by depositing 7075 Al onto the CP Al layer. The effect of carrier gas on the deposit microstructure was also investigated by spraying the same number of passes of CP Al or 7075 Al with N_2 and He.

Microstructure

The deposits were sectioned, mechanically polished, and some were further ion-polished (JEOL SM-09010, Tokyo,

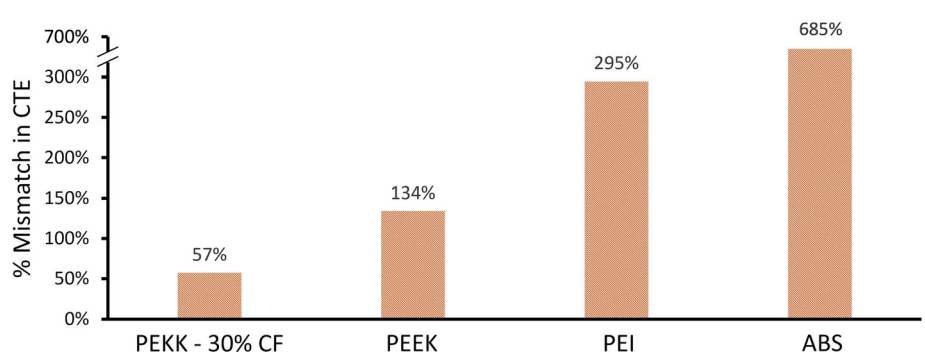

Fig. 1 % Mismatch in coefficient of thermal expansion (CTE) between polymeric substrates and Al (Ref 27). % Mismatch is calculated by the absolute difference in CTE divided by the CTE of Al

Japan). The ion polishing process yielded no surface damage, which rendered the samples suitable for in-depth microstructure characterization through scanning electron microscopy (SEM, JSM-7001F, JEOL Ltd., Tokyo, Japan), energy-dispersive x-ray spectroscopy (EDS, Apollo X SDD, EDAX, Mahwah, NJ, USA.), and electron backscatter diffraction (EBSD, Hikari, EDAX, Mahwah, NJ, USA.) at an acceleration voltage of 15 kV and a working distance of 15 mm. SEM imaging revealed the overall coating quality, EDS exhibited the microstructural features at the deposit–substrate interface, and EBSD yielded the grain structures of the coatings. SEM cross sections were analyzed for coating porosity and interface root-mean-square roughness, which were reported as the average of ten and three calculations (using ImageJ and MATLAB). EBSD maps were analyzed for grain size distributions and aspect ratios using Orientation Imaging Microscopy (OIM) Analysis (EDAX, Mahwah, NJ, USA.).

Mechanical Properties

The adhesive strength of the Al deposit on the substrate was measured per ASTM D4541 using a portable tensile testing instrument (PosiTest AT-M, DeFelsko, Ogdensburg, NY, USA) (Ref 28) and reported as an average of three measurements. A 10-mm-diameter Al pull-stub was bonded to the deposit surface and pulled at a rate of ~0.7-1 MPa per second until deposit–substrate separation or adhesive failure.

Results and Discussion

Microstructure

Figure 2 shows polished sections of the CP Al and 7075 Al deposits, revealing low porosity (< 2%). First, CP Al was deposited onto FRTP via HP-CS using N_2 as the carrier gas. The resultant deposit is shown in Fig. 2(a). The deposit porosity was < 1%, and the thickness was 2.7 mm. Based on these results, CP Al was selected for a bond layer between the composite substrate and the 7075 Al deposit.

Figure 2(b), (c), (d), and (e) shows the microstructures of 7075/CP Al deposits produced with N_2 and He. The deposits exhibit a barely distinguishable overlayer–bond layer interface (highlighted with dashed line) and a deposit–substrate interface similar to Fig. 2(a). Regardless of carrier gas used, the 7075 Al overlayer and CP Al bond layer were in intimate contact with negligible porosity (< 1%), as shown in Fig. 2(b) and (c). The porosity was uniformly distributed in CP Al, similar to Fig. 2(a), except the uppermost CP Al deposit which experienced more compaction from the impinging 7075 Al particles. When He was used as the carrier gas, material mixing occurred at the 7075/CP Al interface, because He yields greater particle impact velocities than N_2 (Ref 29).

Figure 2(d) and (e) shows CP Al particles anchored in the composite substrate, forming the bond layers with some interface roughening and porosity. The images indicate the impinging particles interact differently with the FRTP substrate than with deposited particles. No substrate cracking or distortion was observed, despite the apparent roughening of the FRTP surface. In contrast, prior studies indicated that CS of CP Al onto neat polymer substrates caused both substrate distortion and cracking, attributed to CTE mismatch and low impact strength (Ref 19, 27). He carrier gas in place of N_2 yielded greater impact velocities, resulting in greater roughness (RMS 15.3 μm versus 10.5 μm) at the bond layer–substrate interface.

The greater impact velocity of He led to deposit erosion, as well as greater porosity in the CP Al bond layer. As shown in Table 1, the thickness results were in this order: 7075/CP Al-N_2 > 7075/CP Al-He. This trend is attributed to the erosion caused by the harder 7075 Al particles and the use of He. Instead of effectively compacting the CP Al bond layer, the use of He in place of N_2 as the carrier gas caused erosion and contributed to greater porosity in the bond layer (1.82% versus 0.67%). At greater impact velocities, weakly bonded particles can be dislodged and expelled or trapped in the deposit, but weakly attached, augmenting porosity (Ref 4, 30, 31). The greater impact velocity also drove CP Al deposits deeper into the substrate, causing more interface roughness. Because of the significant metal–metal peening effect, 7075 Al deposits (< 0.1%) exhibited less porosity than CP Al deposits.

Figure 3 shows SEM images and the corresponding EDS maps from the deposit–substrate interface of different combinations; Fig. 3(a), (b), and (c), CP Al-N_2; Fig. 3(d), (e), and (f), 7075/CP Al-N_2; and Fig. 3(g), (h), and (i), 7075/CP Al-He. The EDS maps of Al reveal what appear to be porous or unbonded regions between particles near the substrate, indicated by white arrows in Fig. 3(b), (e), and (h). However, EDS maps of carbon demonstrate that these regions are in fact polymer material displaced from the substrate (Fig. 3(c, f, i)). The network of polymer debris between particles was generated by polymer extruded/dislodged from the substrate by penetrating particles (Ref 1, 15, 25). These particles appear to be equiaxed and show no sign of flattening/SPD. Comparing the He- and N_2-sprayed samples, the He sample exhibited greater roughness (15.3 μm versus 10.5 μm) at the Al–composite interface because of greater particle velocities. As a consequence of hard particle/soft substrate interaction, more polymer was displaced at the deposit–substrate interface in samples sprayed with He. This observation is consistent with previous studies that showed that greater particle

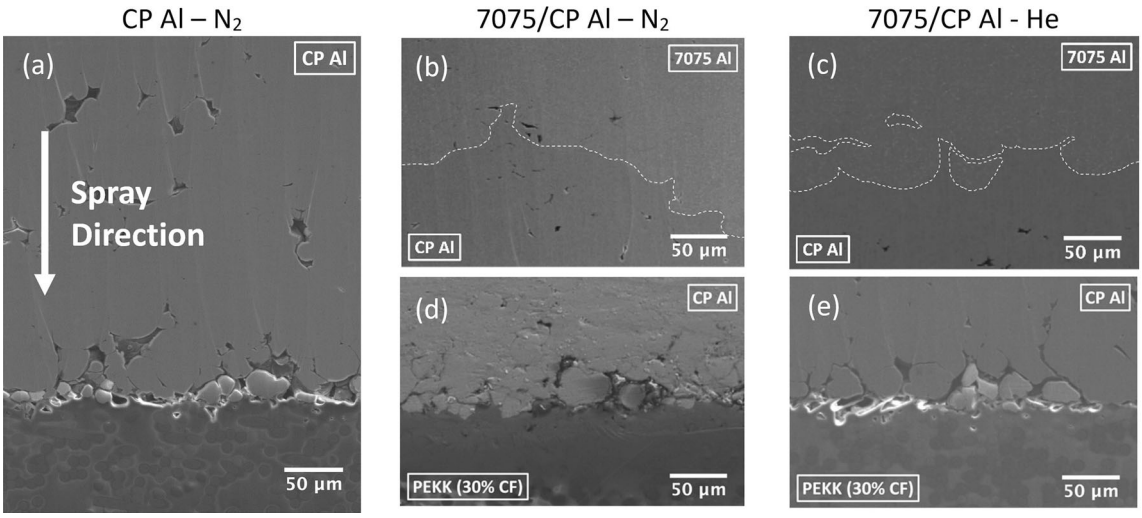

Fig. 2 Cross sections of (a) CP Al-N_2, (b, d) 7075/CP Al-N_2, and (c, e) 7075/CP Al-He. The white dashes in (b, c) outline the interface between 7075 and CP Al layers

Table 1 Coating thickness and porosity

	Thickness (mm)			Porosity (% Area)	
	CP Al	7075 Al	Overall coating	CP Al	7075 Al
CP Al-N_2	2.7	n/a	2.7	0.63	n/a
7075/CP Al-N_2	1.2	0.9	2.1	0.67	0.03
7075/CP Al-He	0.8	0.7	1.5	1.82	0.02

velocities resulted in more severe plastic deformation of the substrate (Ref 32). The network of polymer ligaments prevents intimate contact between particles near the substrate, inhibiting particle bonding and mechanical anchoring of the first few particle layers.

To confirm the presence of the polymer debris network shown in EDS maps, EDS point scans are also carried out. In Fig. 4, the sites labeled 1-4 serve as reference points for the Al deposit and the C-based substrate, and the sites labeled A-E point toward materials mixing features and the polymer debris network. The atomic percent of C and Al at sites labeled in Fig. 4 is shown in Table 2. The C and Al atomic percent in the polymer regions ranges from ~ 20 to 80% for both samples, confirming the presence of a polymer debris network at the deposit–substrate interface. This finding supports the observation in Fig. 3, which shows intermixing of equiaxed particles and polymer displaced ~50 µm from the substrate surface.

Figure 5 shows EBSD orientation maps of interfaces between the first few layers of particles and the substrate deposited with N_2 and He. The high- and low-angle boundaries are outlined in black and white, respectively. The maps show that regardless of carrier gas, the first few layers of particles were not severely deformed and showed no signs of the pancake geometry characteristic of most CS deposits, indicating that particles had not undergone SPD. The relatively mild deformation of particles impinging on the substrate indicates that bonding was most likely weaker at the bond layer–substrate interface than in the subsequently deposited material.

Thermal softening of the substrate caused by the applied carrier gas temperature increased substrate compliance and accommodation of impinging particles. Figure 6(a) and (b) shows that the grain size distributions of the N_2- and He-sprayed samples were comparable (areal average 14.0 µm versus 16.4 µm). Figure 6(c) and (d) shows that the grain aspect ratios were also comparable among the N_2- and He-sprayed samples (number average 0.4 versus 0.4). The carrier gas and the impacting particles can reportedly raise the substrate temperature to $\sim T_g$ (T_g for PEKK = 162 °C), effectively reducing stiffness (increasing compliance) and "cushioning" the incoming particles (Ref 15, 20, 21). Such thermal softening of the substrate reduced the extent of deformation of particles at the substrate and reduced the effects of carrier gas and impact velocity at the interface.

Adhesion

Adhesion tests were conducted to determine the strength of bonding to the composite substrates. Figure 7 shows plan views and cross sections of fractured CP Al-N_2 and

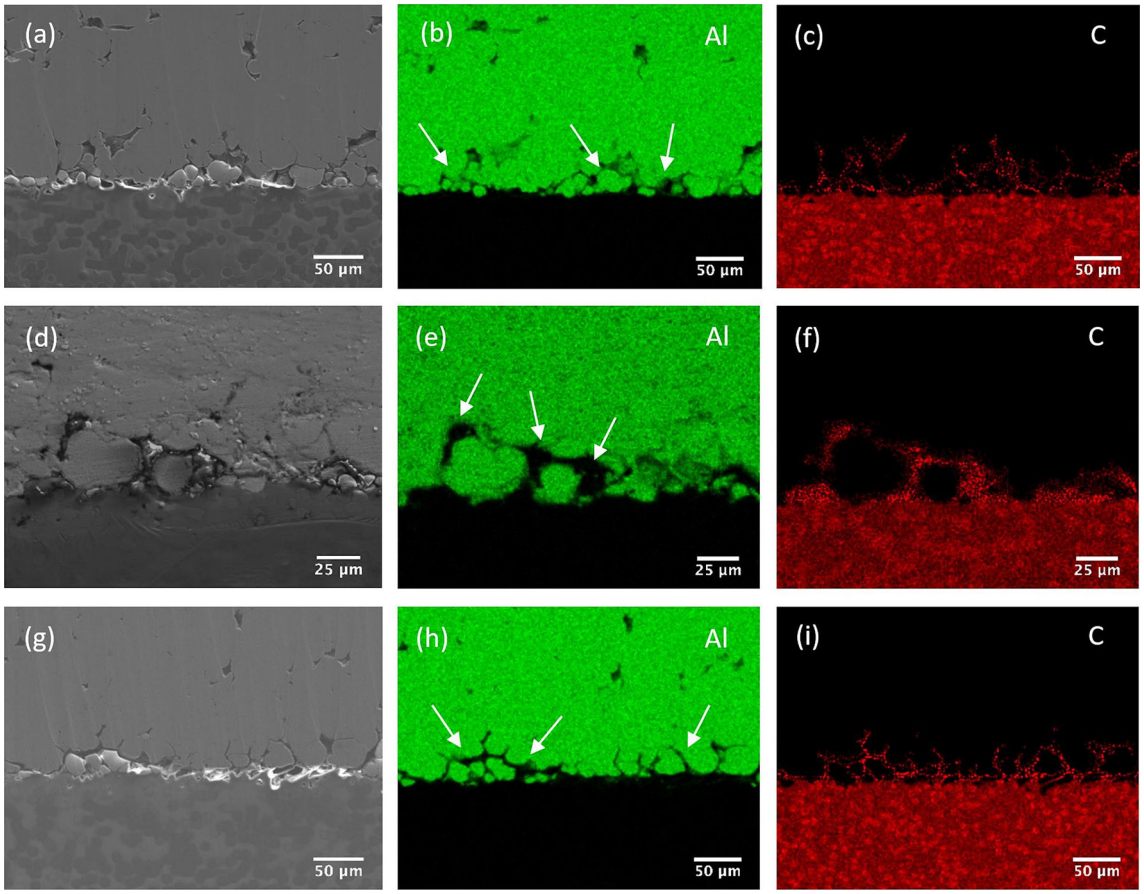

Fig. 3 SEM and EDS (Al, C) images of (a-c) CP Al-N_2, (d-f) 7075/CP Al-N_2, and (g-i) 7075/CP Al-He

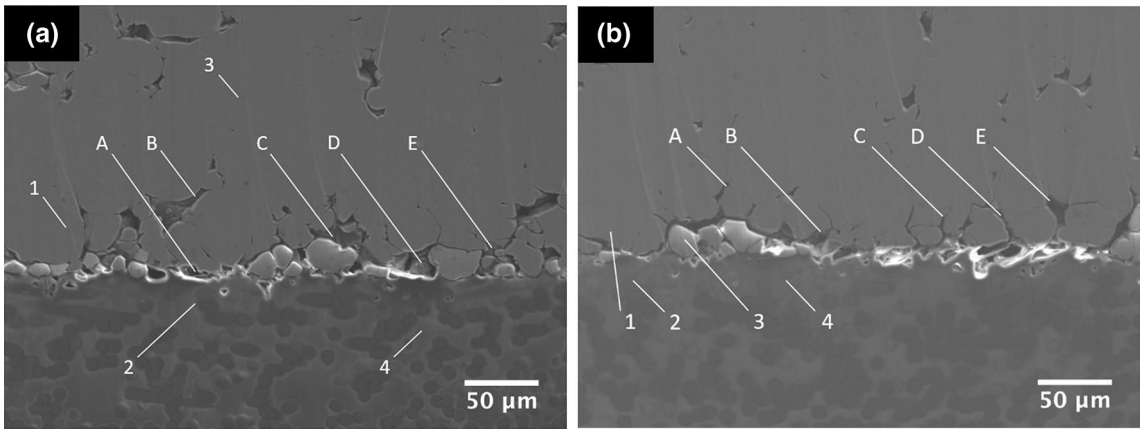

Fig. 4 EDS point scans at the deposit–substrate interface of (a) CP Al-N_2 and (b) 7075/CP Al-He

7075/CP Al-He after adhesion testing. Figure 7(a) and (b) shows comparable gray regions covering the entire cold-sprayed area on the black substrates. These gray regions were metallic residue remaining on the substrate after adhesion testing. Figure 7(c) and (d) shows scattered particles and trapped polymer debris between particles on the substrate, revealing predominantly adhesive failure. Similar findings were previously reported with cold-sprayed Cu onto PEEK (Ref 32). The remaining particles on the substrate were either enclosed by the polymer network (Fig. 3), which prevented contact with the rest of the deposit, or they did not undergo sufficient deformation to fuse with the rest of the deposit (Fig. 5). Although the process yielded thick deposits with little porosity, this failure mode indicates that the first layers of particles were not strongly bonded to the substrate. Compared to the N_2-

sprayed sample, the He-sprayed sample exhibited a more highly textured substrate interface (15.3 µm versus 10.5 µm in roughness), resulting in more dislodged polymer debris between particles. The use of two separate CS recipes—one for the initial layers and a different one for the build-up layers—may produce greater adhesion between the coating and the substrate, as well as between particles.

The adhesive strength values from the current and previous study (CP Al/PEEK-N_2) are compared in Table 3 (Ref 19). Among the N_2-sprayed samples, the substrate choice of PEKK-30% CF versus PEEK resulted in a greater adhesive strength (18.3 MPa vs 11.7 MPa). Although not proven here, a closer match in CTE values between the metal deposit and the polymer substrate may contribute to stronger bonding for metal/composite combinations (Fig. 1). Previous studies have deduced similar connections between the effects of CTE mismatch and associated thermal stresses at the interface, and weaker adhesion (Ref 33, 34). Using a substrate of PEKK-30% CF, deposits sprayed with N_2 instead of He led to greater adhesive strength (18.3 MPa vs 9.3 MPa). This finding can be attributed to He-spraying causing more substrate roughening and generating more polymer debris at the interface, as described in the prior section. Therefore, the carrier gas choice of N_2 and a close deposit–substrate CTE match may both contribute to greater adhesive strength levels.

Table 2 C and Al in at.% with reference to sites labeled in Fig. 4

Atomic%					
CP Al-N_2	C	Al	7075/CP Al-He	C	Al
1	0	100	1	0	100
2	99.64	0.36	2	99.84	0.16
3	0	100	3	0	100
4	99.81	0.19	4	99.70	0.30
A	58.88	41.12	A	72.38	27.62
B	19.84	80.16	B	27.46	72.54
C	26.88	73.12	C	42.22	57.78
D	24.85	75.15	D	62.95	37.05
E	21.66	78.34	E	36.59	63.41

Conclusions

The feasibility of metallizing short fiber composites using HP-CS and a CP Al bond layer was demonstrated. Dense (< 2%area porosity) aluminum deposits (up to 2.7 mm thick) were produced on PEKK-30% CF, and adhesive strengths up to 18.3 MPa were achieved. Closer metal–substrate CTE match increased the coating–substrate adhesive strength compared to previous results (Ref 19). With a fixed CS process, the adhesive strength was governed primarily by the microstructure of the deposit–substrate interface. The choice of carrier gas directly influenced the amount of interface roughening and polymer debris in between particles.

Metal–substrate adhesion can be increased through interface engineering. In the current state, the adhesive strength obtained can fulfill the requirements only for less demanding applications, such as rain erosion protection for wind turbine blades (Ref 35) or corrosion protection for offshore wind power constructions (Ref 36). By tailoring the degree of mechanical interlocking and particle deformation at the deposit–substrate interface, cold spray can produce an adherent metal overlayer. This metal base layer can be used to introduce coating technologies, originally only applicable to metal substrates, to polymer and composites, and in turn expand the use of cold spray to not only

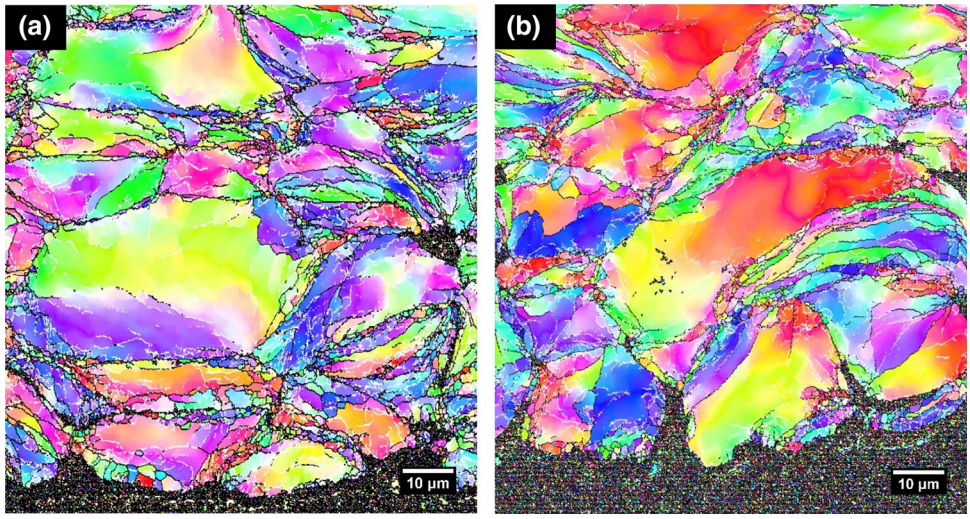

Fig. 5 EBSD images showing the CP Al/PEKK-30% CF interface of (a) CP Al-N_2 and (b) 7075/CP Al-He

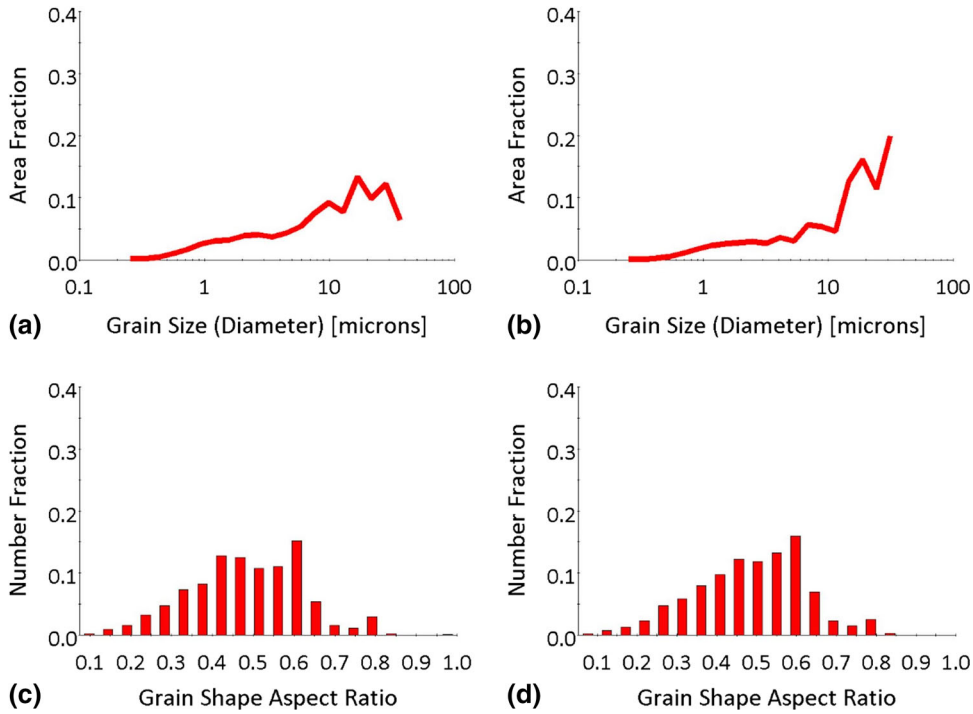

Fig. 6 Grain size (a, b) and aspect ratio distributions (c, d) of CP Al-N_2 and 7075/CP Al-He at the deposit–substrate interface, respectively

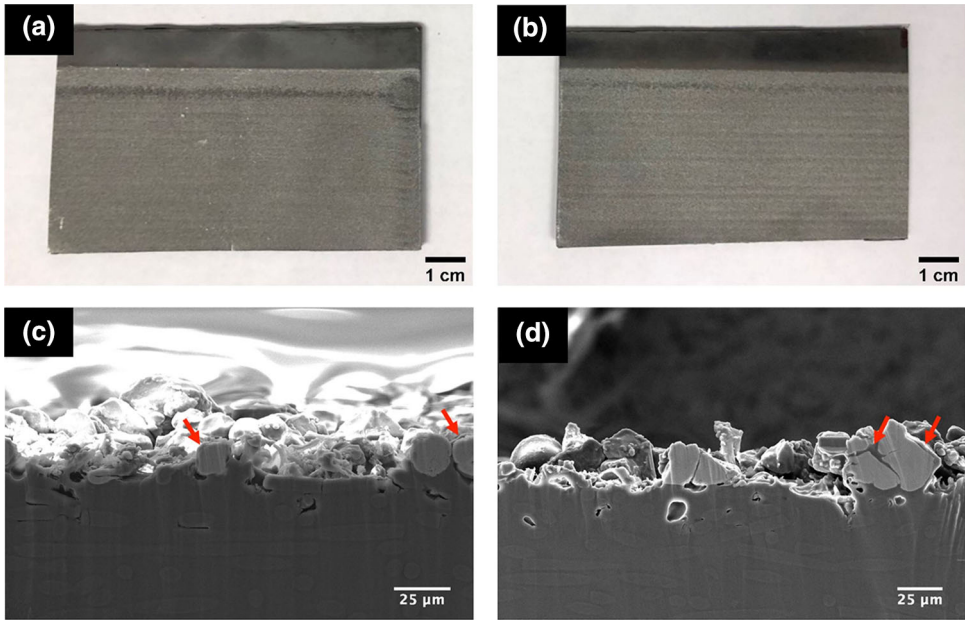

Fig. 7 Plan views and cross sections of (a, c) CP Al-N_2 and (b, d) 7075/CP Al-He substrate after adhesion testing. The arrows point toward the trapped polymer debris between particles

Table 3 Adhesive strength between coating and substrate

Combination	CP Al/PEEK-N_2	CP Al/PEKK (30% CF)-N_2	7075/CP Al/PEKK (30% CF)-He
Adhesive strength (MPa)	11.7	18.3	9.3

repair, coating, additive manufacturing, but also manufacturing processes for metal–polymer hybrid structures.

Acknowledgments The authors acknowledge financial support from Concepts to Systems, Inc. (Dr. Shiv Joshi, PI) through an SBIR contract supported by the US Army (W9113M-18-C-0014). The authors also thank Dr. Marius Ellingsen of VRC Metal Systems for cold-spraying samples and fulfilling custom requests in a timely fashion.

References

1. A. Ganesan, J. Affi, M. Yamada, and M. Fukumoto, Bonding Behavior Studies of Cold Sprayed Copper Coating on the PVC Polymer Substrate, *Surf. Coat. Technol.*, 2012, **207**, p 262-269.
2. A.S. Perna, A. Viscusi, A. Astarita, L. Boccarusso, L. Carrino, M. Durante, and R. Sansone, Manufacturing of a Metal Matrix Composite Coating on a Polymer Matrix Composite Through Cold Gas Dynamic Spray Technique, *J. Mater. Eng. Perform.*, 2019, https://doi.org/10.1007/s11665-019-03914-6
3. H. Che, M. Gagné, P.S.M. Rajesh, J.E. Klemberg-Sapieha, F. Sirois, D. Therriault, and S. Yue, Metallization of Carbon Fiber Reinforced Polymers for Lightning Strike Protection, *J. Mater. Eng. Perform.*, 2018, **27**(10), p 5205-5211.
4. A. Viscusi, A. Astarita, R. Della Gatta, F. Rubino, A Perspective Review on the Bonding Mechanisms in Cold Gas Dynamic Spray, *Surf. Eng.*, 2019, **0844**, p 743–771.
5. B. Fotovvati, N. Namdari, and A. Dehghanghadikolaei, On Coating Techniques for Surface Protection: A Review, *J. Manuf. Mater. Process.*, 2019, **3**(1), p 28.
6. Y.J. Yim, K.Y. Rhee, and S.J. Park, Influence of Electroless Nickel-Plating on Fracture Toughness of Pitch-Based Carbon Fibre Reinforced Composites, *Compos. Part B Eng.*, 2015, **76**, p 286-291. https://doi.org/10.1016/j.compositesb.2015.01.052
7. M. Ivosevic, R. Knight, S.R. Kalidindi, G.R. Palmese, and J.K. Sutter, Adhesive/Cohesive Properties of Thermally Sprayed Functionally Graded Coatings for Polymer Matrix Composites, *J. Therm. Spray Technol.*, 2005, **14**(1), p 45-51.
8. R. Gonzalez, H. Ashrafizadeh, A. Lopera, P. Mertiny, and A. McDonald, A Review of Thermal Spray Metallization of Polymer-Based Structures, *J. Therm. Spray Technol.*, 2016, **25**(5), p 897-919.
9. J. Villafuerte, *Modern Cold Spray: Materials, Process, and Applications* (Springer, Berlin, 2015). https://doi.org/10.1007/978-3-319-16772-5.
10. P. Cavaliere, *Cold-Spray Coatings: Recent Trends and Future Perspectives* (Springer, Berlin, 2015). https://doi.org/10.1007/978-3-319-67183-3.
11. X.L. Zhou, A.F. Chen, J.C. Liu, X.K. Wu, and J.S. Zhang, Preparation of Metallic Coatings on Polymer Matrix Composites by Cold Spray, *Surf. Coat. Technol.*, 2011, **206**(1), p 132-136.
12. F. Robitaille, M. Yandouzi, S. Hind, and B. Jodoin, Metallic Coating of Aerospace Carbon/Epoxy Composites by the Pulsed Gas Dynamic Spraying Process, *Surf. Coat. Technol.*, 2009, **203**(19), p 2954-2960.
13. R. Lupoi and W. O'Neill, Deposition of Metallic Coatings on Polymer Surfaces Using Cold Spray, *Surf. Coat. Technol.*, 2010, **205**(7), p 2167-2173.
14. V. Champagne and D. Helfritch, The Unique Abilities of Cold Spray Deposition, *Int. Mater. Rev.*, 2016, **61**(7), p 437-455.
15. A. Ganesan, M. Yamada, and M. Fukumoto, Cold Spray Coating Deposition Mechanism on the Thermoplastic and Thermosetting Polymer Substrates, *J. Therm. Spray Technol.*, 2013, **22**(8), p 1275-1282.
16. P.C. King, A.J. Poole, S. Horne, R. de Nys, S. Gulizia, and M.Z. Jahedi, Embedment of Copper Particles into Polymers by Cold Spray, *Surf. Coat. Technol.*, 2013, **216**, p 60-67.
17. C. Stenson, K.A. McDonnell, S. Yin, B. Aldwell, M. Meyer, D.P. Dowling, and R. Lupoi, Cold Spray Deposition to Prevent Fouling of Polymer Surfaces, *Surf. Eng.*, 2018, **34**(3), p 193-204.
18. H. Che, P. Vo, and S. Yue, Metallization of Various Polymers by Cold Spray, *J. Therm. Spray Technol.*, 2018, **27**(1–2), p 169-178.
19. M.R. Rokni, P. Feng, C.A. Widener, and S.R. Nutt, Depositing Al-Based Metallic Coatings onto Polymer Substrates by Cold Spray, *J. Therm. Spray Technol.*, 2019, https://doi.org/10.1007/s11666-019-00911-y
20. H. Che, P. Vo, and S. Yue, Investigation of Cold Spray on Polymers by Single Particle Impact Experiments, *J. Therm. Spray Technol.*, 2019, **28**(1–2), p 135-143. https://doi.org/10.1007/s11666-018-0801-4
21. M. Gardon, A. Latorre, M. Torrell, S. Dosta, J. Fernández, and J.M. Guilemany, Cold Gas Spray Titanium Coatings onto a Biocompatible Polymer, *Mater. Lett.*, 2013, **106**, p 97-99. https://doi.org/10.1016/j.matlet.2013.04.115
22. V. Bortolussi, B. Figliuzzi, F. Willot, M. Faessel, and M. Jeandin, Electrical Conductivity of Metal-Polymer Cold Spray Composite Coatings onto Carbon Fiber-Reinforced Polymer, *J. Therm. Spray Technol.*, 2020, **29**(4), p 642-656.
23. A. Małachowska, M. Winnicki, M. Stachowicz, and M. Korzeniowski, Metallisation of Polycarbonates Using a Low Pressure Cold Spray Method, *Surf. Eng.*, 2018, **34**(3), p 251-258.
24. A. Astarita, L. Boccarusso, M. Durante, A. Viscusi, R. Sansone, and L. Carrino, Study of the Production of a Metallic Coating on Natural Fiber Composite Through the Cold Spray Technique, *J. Mater. Eng. Perform.*, 2018, **27**(2), p 739-750.
25. I. Burlacov, J. Jirkovský, L. Kavan, R. Ballhorn, and R.B. Heimann, Cold Gas Dynamic Spraying (CGDS) of TiO2 (Anatase) Powders onto Poly(Sulfone) Substrates: Microstructural Characterisation and Photocatalytic Efficiency, *J. Photochem. Photobiol. A Chem.*, 2007, **187**(2–3), p 285-292.
26. J. Affi, H. Okazaki, M. Yamada, and M. Fukumoto, Fabrication of Aluminum Coating onto CFRP Substrate by Cold Spray, *Mater. Trans.*, 2011, **52**(9), p 1759-1763.
27. Granta Design, "CES EduPack," *Granta Design*, 2019.
28. ASTM D4541-17, Standard Test Method for Pull-Off Strength of Coatings Using Portable Adhesion, *ASTM Int*, 2017.
29. M. Grujicic, C.L. Zhao, C. Tong, W.S. DeRosset, and D. Helfritch, Analysis of the Impact Velocity of Powder Particles in the Cold-Gas Dynamic-Spray Process, *Mater. Sci. Eng. A*, 2004, **368**(1–2), p 222-230.
30. N. Cinca, M. Barbosa, S. Dosta, and J.M. Guilemany, Study of Ti Deposition onto Al Alloy by Cold Gas Spraying, *Surf. Coat. Technol.*, 2010, **205**(4), p 1096-1102.
31. S. Adachi and N. Ueda, Effect of Cold-Spray Conditions Using a Nitrogen Propellant Gas on AISI 316L Stainless Steel-Coating Microstructures, *Coatings*, 2017, **7**(7), p 3-11.
32. C. Chen, X. Xie, Y. Xie, X. Yan, C. Huang, S. Deng, Z. Ren, and H. Liao, Metallization of Polyether Ether Ketone (PEEK) by Copper Coating via Cold Spray, *Surf. Coat. Technol.*, 2018, **342**(1), p 209-219. https://doi.org/10.1016/j.surfcoat.2018.02.087
33. Y. Xiong, W. Zhuang, and M. Zhang, Effect of the Thickness of Cold Sprayed Aluminium Alloy Coating on the Adhesive Bond Strength with an Aluminium Alloy Substrate, *Surf. Coat. Technol.*, 2015, **270**, p 259-265. https://doi.org/10.1016/j.surfcoat.2015.02.048
34. Y. Watanabe, C. Yoshida, K. Atsumi, M. Yamada, and M. Fukumoto, Influence of Substrate Temperature on Adhesion Strength of Cold-Sprayed Coatings, *J. Therm. Spray Technol.*, 2014, **24**(1–2), p 86-91.

35. E. Cortés, F. Sánchez, A. O'Carroll, B. Madramany, M. Hardiman, and T.M. Young, On the Material Characterisation of Wind Turbine Blade Coatings: The Effect of Interphase Coating-Laminate Adhesion on Rain Erosion Performance, *Materials (Basel)*, 2017, **10**(10), p 1146.
36. A.W. Momber, P. Plagemann, and V. Stenzel, The Adhesion of Corrosion Protection Coating Systems for Offshore Wind Power Constructions after Three Years under Offshore Exposure, *Int. J. Adhes. Adhes.*, 2016, **65**, p 96-101. https://doi.org/10.1016/j.ijadhadh.2015.11.011